

## Effect of growth conditions on microstructure of BiFeO<sub>3</sub>-0.33BaTiO<sub>3</sub> films and performance of bulk acoustic wave resonators

A. Vorobiev,<sup>1,a)</sup> M. Löffler,<sup>2,b)</sup> E. Olsson,<sup>2</sup> and S. Gevorgian<sup>1</sup>

<sup>1</sup>*Department of Microtechnology and Nanoscience, Chalmers University of Technology, SE-41296 Gothenburg, Sweden*

<sup>2</sup>*Department of Applied Physics, Chalmers University of Technology, SE-41296 Gothenburg, Sweden*

(Received 28 January 2014; accepted 8 February 2014; published online 25 February 2014)

The effect of growth conditions on the microstructure of BiFeO<sub>3</sub>-0.33BaTiO<sub>3</sub> (BF-BT) films and the performance of bulk acoustic wave (BAW) resonators is analyzed using test structures with the BF-BT films grown at different positions relative to the plume axis in the pulsed laser deposition system. The BF-BT film grain size and surface roughness reveal a strong asymmetric surface distribution and decrease significantly in the film region facing the laser beam-plume interaction area. The (100) BF-BT texturing is enhanced in this film region. The variations in the BF-BT film microstructure result in corresponding variations of the BAW resonator performance. Their correlations are established using the model of the roughness induced attenuation of the reflected acoustic waves and theory of the dc field induced piezoelectric effect. The BAW resonators with the highest parameters are obtained in the BF-BT film region facing the laser beam-plume interaction area. The BAW resonators located in this film region reveal a mechanical  $Q$ -factor of 200 at 4.2 GHz, an effective electromechanical coupling coefficient of 10% and a tunability of the series resonance frequency of 4.5%. © 2014 AIP Publishing LLC. [<http://dx.doi.org/10.1063/1.4866420>]

### I. INTRODUCTION

The intrinsically tunable thin film bulk acoustic wave (BAW) resonators, based on the electric field induced piezoelectric effect in ferroelectrics have been intensively developed for the last few years.<sup>1–7</sup> They offer great opportunities for the development of novel reconfigurable/adaptable microwave circuit architectures. However, the tunability of the resonance frequency and effective electromechanical coupling coefficient of the reported BAW resonators are still lower than required. For applications in agile front ends of advanced transceivers of microwave communication systems, the tunability of the BAW resonators should be more than 5%. The required coupling coefficient is defined by the system bandwidth and, for example, in personal communication systems should be 6% and higher.<sup>8</sup> Intrinsically tunable 0.67BiFeO<sub>3</sub>-0.33BaTiO<sub>3</sub> (BF-BT) thin film BAW resonators with record high tunability of series resonance frequency of 4.4%, effective electromechanical coupling coefficient of 10% and a rather high mechanical  $Q$ -factor of 200, at 4 GHz, have been demonstrated recently.<sup>9</sup> The BF-BT films are grown by the pulsed laser deposition (PLD) technique. The achieved high tunability of the resonance frequency and effective electromechanical coupling coefficient are associated with intrinsically high values of components of the tensor of linear electrostriction of the BF-BT material.<sup>9</sup> The relatively high  $Q$ -factor is achieved by minimizing the BF-BT film surface roughness via an optimization of the substrate position in the PLD system with respect to the laser plume axis.<sup>9</sup> In this paper, we disclose details of the optimization and effect of the

substrate position on the BF-BT film microstructure and the BAW resonator performance.

In any PLD system, the laser beam is partly absorbed by the plume plasma before it reaches the target surface, which is so-called “plasma shielding” effect. Simulations show that even for short laser pulses with duration of 5 ns, the fraction of laser energy absorbed by the plume can be up to 50%.<sup>10</sup> The absorption of the laser beam increases the plasma temperature in the part of the plume which absorbs the laser beam.<sup>10</sup> This should result in local modification of the plume parameters, in particular, flow velocity and, hence, energy of species arriving at condensation surface. In the PLD systems of the conventional configuration, the laser beam-plume interaction area is located asymmetrically with respect to the plume axis. Therefore, one can expect an asymmetric distribution of the film properties over the condensation surface. The asymmetric surface distribution of the PLD film properties is not a well-known phenomenon. We assume that the distribution of the energy of the ablated species results in distribution of the mobility of adparticles and, hence, the distribution of the lateral sizes of the film grains.<sup>11</sup> Variations in the lateral grain size cause variations in the film surface roughness if the latter is defined mainly by the shape of the faceted grain tips.<sup>11</sup> The film surface roughness is responsible for the main extrinsic acoustic loss mechanism in the ferroelectric BAW resonators associated with wave scattering at reflection from a rough interface.<sup>7,12,13</sup> Thus, an asymmetric distribution of the  $Q$ -factors of the BAW resonators with respect to the plume axis is expected. Additionally, the surface distribution of the energy of the adparticles can alter the surface distribution of the grain orientation, i.e., texturing, if the growth rate in a certain crystallographic direction is governed by the lowest free surface energy.<sup>14</sup> Consequently, texturing results in strong surface distribution of the tunabilities

<sup>a)</sup>Electronic mail: andrei.vorobiev@chalmers.se

<sup>b)</sup>Present address: TU Dresden, Dresden Center for Nanoanalysis, Dresden 101062, Germany.

and coupling coefficients of the BAW resonators because of the inherent anisotropy of the components of the tensors of linear and nonlinear electrostriction.<sup>13,15</sup>

In this paper, we demonstrate variations of the BF-BT film microstructure with position on the condensation surface in the PLD system relative to the laser beam-plume interaction area. Analysis of the correlations between the BF-BT film microstructure and the acoustic performance of the BAW resonators allows for an optimization of the PLD system configuration and achieving the high resonator performance.

## II. EXPERIMENTAL DETAILS

The BF-BT BAW resonator test structures are fabricated as solidly mounted resonators on silicon substrates with resistivity of  $20 \text{ k}\Omega \cdot \text{cm}$ . The Bragg reflector, consisting of  $\lambda/4$   $\text{SiO}_2/\text{W}$  layers with thicknesses of 280/240 nm, and 100 nm Pt bottom plate are deposited by magnetron sputtering. The 50/10 nm thick  $\text{TiO}_2/\text{Ti}$  diffusion barrier/adhesion layer stacks are deposited below the Pt bottom plate. The BF-BT films are grown in a PLD system using a 0.1 wt. %  $\text{MnO}_2$  doped  $0.67\text{BiFeO}_3\text{-}0.33\text{BaTiO}_3$  target. The target is ablated by a KrF excimer laser beam with wavelength of 248 nm, pulse duration of 30 ns and repetition rate of 10 Hz, focused in a spot of  $1 \times 4 \text{ mm}^2$ , which results in energy density of  $1.5 \text{ J/cm}^2$ . The BF-BT films are grown in oxygen ambient at pressure of 0.4 mbar. The substrate temperature is maintained at  $650^\circ\text{C}$ . The Al top electrodes with Ti adhesion layers are deposited by e-beam evaporation. A lift-off process is used to pattern the top electrodes in the form of  $60 \mu\text{m}$  in diameter central circular patches surrounded by concentric outer electrodes with inner diameter of  $200 \mu\text{m}$ . The cross-sectional structure and layout of the BAW resonator test structures are similar to those shown in Ref. 16. The BAW resonator test structures are distributed evenly over the whole surface of the  $10 \times 10 \text{ mm}^2$  sample chips.

The microstructure of the BF-BT films and resonator multilayer stacks is analyzed using X-ray diffraction (XRD), scanning electron microscopy (SEM) and atomic force microscopy (AFM) techniques. The XRD spectra are obtained using a Philips X'pert SW 3040 diffractometer equipped with a point  $\text{Cu K}_\alpha$  radiation source, a PANalytical's X'Pert PRO Materials Research Diffractometers (MRD) lens, a rocking curve detector and a Ni filter. The SEM images of the BF-BT film surface and cross-section are obtained using a Zeiss Ultra SEM. The cross-sections are prepared using a dual-beam focused ion beam/scanning electron microscope FEI Versa. The SEM cross-section images are analyzed using a Mathematica script allowing for the calculation of the rms surface roughness. The SEM surface images are used to determine lateral grain sizes by using the line intercept method.

The complex input impedance  $Z = \text{Re}Z + j\text{Im}Z$  and admittance of test structures are calculated using  $S_{11}$  parameters measured using an Agilent N5230A vector network analyzer and ground-signal-ground microprobes in the frequency range 1–10 GHz. The modified Butterworth-Van Dyke (mBVD) circuit model is used for de-embedding the electrical loss associated with the series resistance  $R_s$  composed by the ring section of the Pt bottom electrode and the

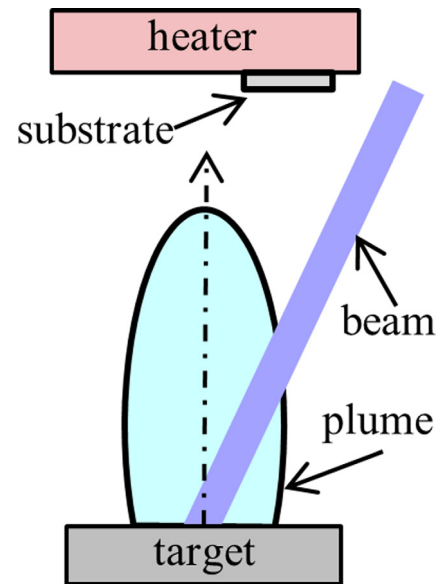


FIG. 1. Schematic diagram of the PLD system. Sample shown is placed in *off-axis* position facing the area of the laser beam-plume interaction.

contact resistance between Al pads and probe tips. The series resistance in the mBVD model is found as the real part of impedance in the high frequency limit.<sup>7</sup>

A schematic diagram of the PLD system is shown in Fig. 1. It was found that the BF-BT film grain size, surface roughness and texturing vary significantly depending on the position of the samples with respect to the laser plume axis. Acoustic performance of the BF-BT BAW resonators varies correspondingly. In particular, BAW resonators with the highest  $Q$ -factor and effective electromechanical coupling coefficient are obtained using the BF-BT films grown in *off-axis* position facing the area of the laser beam-plume interaction, as shown in the Fig. 1. Fig. 2 shows a photo of the PLD heater surface with a sample attached in *off-axis* position after deposition of the BF-BT film. With the aim to establish correlations between the BF-BT film microstructure and the BAW resonator performance two sets of the samples

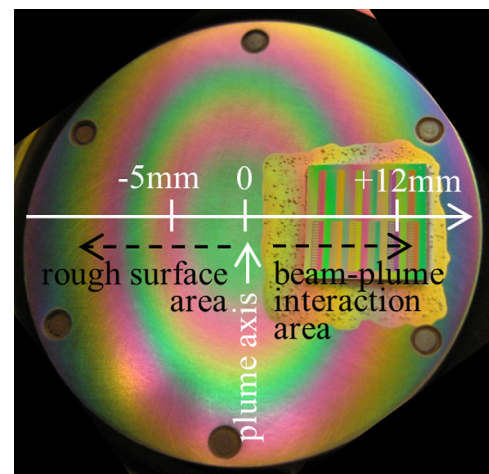


FIG. 2. Photo of PLD heater surface, with a sample attached, after deposition of the BF-BT film. The origin of coordinate system ( $x=0$ ) coincides with the laser plume axis and positive part ( $x>0$ ) faces the laser beam-plume interaction area.

are fabricated and studied with BF-BT films grown in *on-axis* and *off-axis* positions. To analyze the BF-BT film and BAW resonator properties distribution, we define a coordinate system with zero ( $x=0$ ) at the plume axis and positive part ( $x>0$ ) facing the beam-plume interaction area, as shown in Fig. 2. The BF-BT film deposition time in *on-axis* and *off-axis* positions has been adjusted (15 min and 25 min, respectively) with the aim to obtain BAW resonators with similar film thickness. In the analysis below, we consider sets of the BAW resonator test structures placed at three different coordinates  $x = -5, 0$ , and  $+12$  mm. They reveal a similar BF-BT film thickness of 330 nm with deviations less than 10 nm.

### III. RESULTS AND DISCUSSION

#### A. Microstructure

Fig. 3 shows the XRD patterns of the complete BAW resonator multilayer stacks with BF-BT films grown in *on-axis* position and *off-axis* position with positive coordinates  $x$ . The X-ray beam has been located in the center of the samples, which corresponds to coordinates  $x=0$  mm and  $x=+9$  mm for the *on-axis* and *off-axis* samples, respectively. It should be noted that the size of the X-ray beam spot on the sample surface is approximately  $4\text{ mm}^2$ . Therefore, the XRD reflections represent some integral responses of the microstructure of the BF-BT film regions distributed inside the X-ray beam spot. The peak marked as q(011) in Fig. 3 is identified as reflection from the strained cristobalite associated with partly crystallized  $\text{SiO}_2$  layers of the Bragg reflector. The only reflections from the BF-BT (100) and (110) orientations can be observed. The BF-BT (111) reflection is, apparently, masked by strong Pt (111) and W (110) peaks. The comparison with the XRD pattern of the ceramic counterpart (Ref. 17) indicates that the BF-BT films are (100) textured. The texturing ratio is defined as<sup>18</sup>

$$M = \frac{I_{(100)}^f}{I_{(100)}^c} \cdot \frac{I_{(100)}^c + I_{(110)}^c}{I_{(100)}^f + I_{(110)}^f}, \quad (1)$$

where  $I_{(hkl)}^f$  and  $I_{(hkl)}^c$  are the intensities of the (hkl) peaks of the film and ceramic, respectively. Calculations using (1)

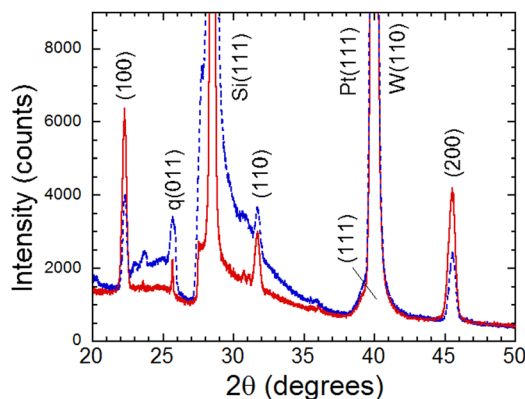


FIG. 3. XRD spectra of the complete BAW resonator multilayer structures with BF-BT films grown in *on-axis* position (dashed line) and *off-axis* position with positive coordinates  $x$  (solid line).

give texturing ratios of 1.82 and 2.39 for the *on-axis* and *off-axis* BF-BT films, respectively. Therefore, one can conclude that the (100) BF-BT texturing is enhanced in the film regions facing the laser beam-plume interaction area.

Fig. 4 shows SEM images of the BF-BT film surfaces obtained at different coordinates  $x = -4, +0.3$ , and  $+12$  mm. It can be seen that the BF-BT film grain size decreases significantly with increasing coordinate  $x$ . The SEM cross-section images reveal a columnar structure of the BF-BT films without a thickness distribution of the column width. Therefore, the effect of the BF-BT film thickness distribution on the grain size can be ignored. Analysis of the SEM surface and cross-section images allows for a calculation of the BF-BT film grain size and rms surface roughness. Fig. 5 shows the BF-BT film grain size and rms surface roughness plotted versus coordinate  $x$ . It can be seen that both the grain size and surface roughness reveal rather strong asymmetric surface distribution decreasing with increasing coordinate  $x$ . It is assumed that the surface roughness is defined by the

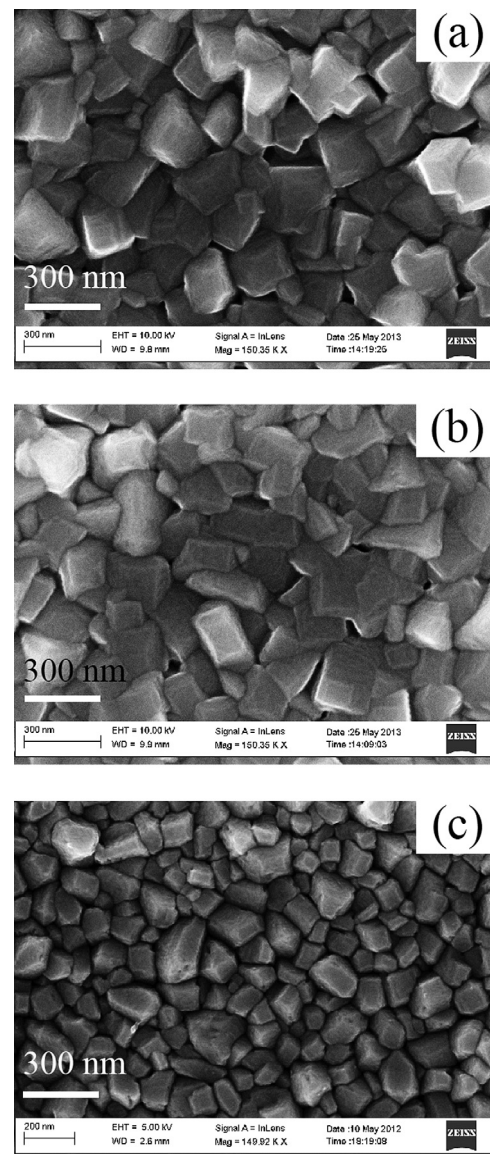


FIG. 4. SEM images of the BF-BT film surfaces obtained at different coordinates  $x$ :  $-4$  mm (a),  $+0.3$  mm (b), and  $+12$  mm (c).

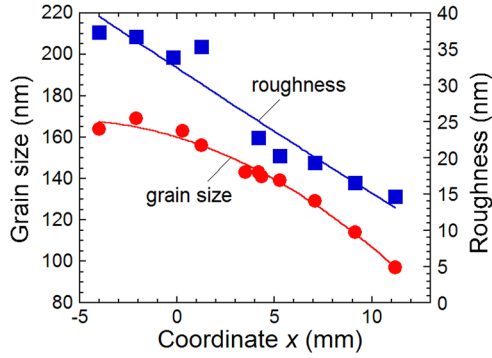


FIG. 5. Grain size and rms surface roughness of the BF-BT films vs. coordinate  $x$ .

faceted grain tips. Therefore, a decrease in the surface roughness is caused by the decrease in the grain size. An additional effect is associated with the grain orientation. Obviously, the (100) oriented grain tips are flat resulting in smooth film surface, while the (110) and (111) oriented grain tips reveal triangular shapes resulting in rougher film surface. Therefore, both reduction in the grain size and stronger (100) texturing are responsible for the smoother surface of the films in regions facing the laser beam-plume interaction area.

The observed strong asymmetric surface distribution of the BF-BT film grain size, surface roughness, and texturing can be associated with a corresponding distribution of energy of the ablated species caused by the laser beam-plume interaction. Calculations performed for a laser beam with similar parameters indicate that even a shorter pulse of 5 ns is partly absorbed by the plume plasma before it reaches the target, which is the so-called “plasma shielding” effect.<sup>10</sup> Consequently, the plume plasma temperature and pressure are higher in the local area of the beam-plume interaction, as shown in Fig. 1, which causes a decrease in the plume flow velocity in this area. It results in asymmetric distribution of the energy of the ablated species arriving at condensation surface. The energy of the species and, hence, the mobility of adparticles in the film regions facing the laser beam-plume interaction area are reduced. The lateral grain size is reduced correspondingly, since it is directly defined by the mobility of the adparticles.<sup>11</sup> The reduced lateral grain size results in a decrease of the film surface roughness if latter is defined mainly by the shape of the grain faceted tips. The surface distribution of the energy of the adparticles can explain also the observed surface distribution of the grain orientation, i.e., texturing, if the growth rate in certain crystallographic direction is governed by the lowest free surface energy.<sup>14</sup>

## B. Resonator performance

The strong asymmetric surface distribution of the BF-BT film grain size, surface roughness, and texturing results in a corresponding distribution of the BAW resonator performance. The highest  $Q$ -factor and coupling coefficient are achieved using the BF-BT films grown in the *off-axis* position, in the “smooth” film region facing the laser beam-plume interaction area. It will be shown below that the  $Q$ -factor in the “rough” film regions is defined mainly by the

BF-BT film surface roughness, which is responsible for extrinsic acoustic loss associated with wave scattering at reflection from rough interfaces. This loss mechanism assumes redirection of vertically moving acoustic waves toward lateral directions. It causes the waves to leave the active resonator region and dissipate either in the device substrate or in the region surrounding the device laterally. Our transmission electron microscopy studies (Ref. 12) indicate that the surface of the top Bragg reflector  $\text{SiO}_2$  layer, which is the main bottom reflecting interface, is relatively smooth. The surface of the top electrode, which is the main top reflecting interface, is significantly rougher. The surface morphology of the top electrode reproduces the surface morphology of the BF-BT film. Therefore, it is assumed that the scattering loss is mainly defined by the BF-BT film surface roughness. Fig. 6 shows the  $Q$ -factor of the BAW resonators for different coordinates  $x$ . The  $Q$ -factor is calculated as

$$Q = \frac{1}{2} f_s \left. \frac{\partial \varphi_{de}}{\partial f} \right|_{f=f_s}, \quad (2)$$

where  $f_s$  is the series resonance frequency determined at the maximum of the real part of the complex admittance and

$$\varphi_{de} = \arctg \frac{\text{Im} Z}{\text{Re} Z - R_s} \quad (3)$$

is the de-embedded phase angle. The de-embedding of the electrical loss allows for considering the  $Q$ -factor calculated using Eq. (2) as the mechanical one. In Fig. 6, the corresponding BF-BT film rms surface roughness is shown in brackets. It can be seen that in the “smooth” film region the  $Q$ -factor is, approximately, 10 times higher. For a single reflection act and lateral roughness scale much smaller than the wavelength, the attenuation coefficient can be approximated in dB as<sup>19</sup>

$$\alpha_{dB} = 2\pi 8.68 k^2 \eta^2 \text{dB}, \quad (4)$$

where  $k = 2\pi/\lambda$  is the longitudinal wave number,  $\lambda$  is the wavelength and  $\eta$  is the rms surface roughness. Using a

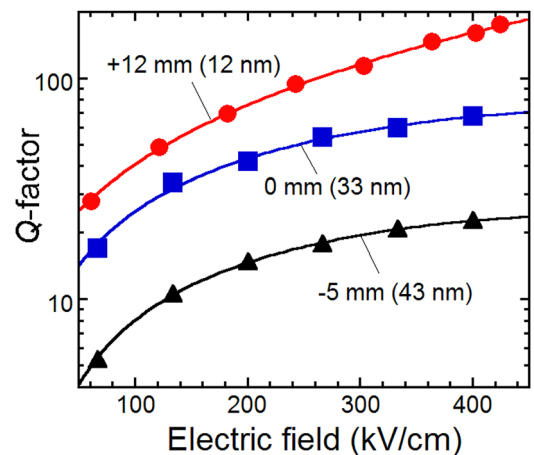


FIG. 6.  $Q$ -factors of the BF-BT BAW resonators vs. applied dc electric field for different coordinates  $x$ . The corresponding rms surface roughness is shown in brackets.

general definition of the  $Q$ -factor as the ratio between energy stored and energy dissipated per cycle, the  $Q$ -factor of the BAW resonator, associated with wave scattering at top interface only, can be calculated as

$$Q_{sc} = 2\pi \frac{E_{tot}}{E_{tot} - E_{ref}} = \frac{2\pi}{1 - \frac{1}{\alpha}}, \quad (5)$$

where  $E_{tot}$  and  $E_{ref}$  represent the energies of incoming and reflected acoustic waves, respectively,  $\alpha = E_{tot}/E_{ref}$  is the attenuation coefficient and  $\log \alpha = 0.1\alpha_{dB}$ . Assuming that the wavelength equals to the double thickness of the ferroelectric film and electrodes  $\lambda = 1060$  nm, using (5) and the measured BF-BT film surface roughness, obtained by the analysis of the SEM cross-section images, one can readily get  $Q$ -factor values of 624, 85, and 52 for the corresponding rms surface roughness of 12 nm, 33 nm, and 43 nm. These simple calculations overestimate the  $Q$ -factor since they take into account only loss at reflection from top interface. However, comparison of the calculated and measured  $Q$ -factor values (Fig. 6) allows for conclusion that in the “rough” film regions the  $Q$ -factor is limited mainly by loss associated with wave scattering at reflection from rough top interface.

Apart from the  $Q$ -factor, the main parameters characterizing BAW resonator performance are the effective electromechanical coupling coefficient and tunability of the resonance frequencies. Below we analyze effect of the BF-BT film texturing on the BAW resonator coupling coefficient and tunability. Fig. 7 shows dc electric field dependences of relative tunability of permittivity of the BF-BT films for different coordinates  $x$ . The relative tunability of permittivity is calculated at 4.2 GHz, which is close to the resonance frequency, as

$$n_r = \frac{\varepsilon(0) - \varepsilon(E)}{\varepsilon(0)}, \quad (6)$$

where  $\varepsilon(0)$  and  $\varepsilon(E)$  are the permittivity without and with dc electric field, respectively. It can be seen that the dependences are practically identical indicating that the observed surface distribution of the BF-BT film grain size, surface roughness and texturing hardly affect the permittivity and its dc field dependence.

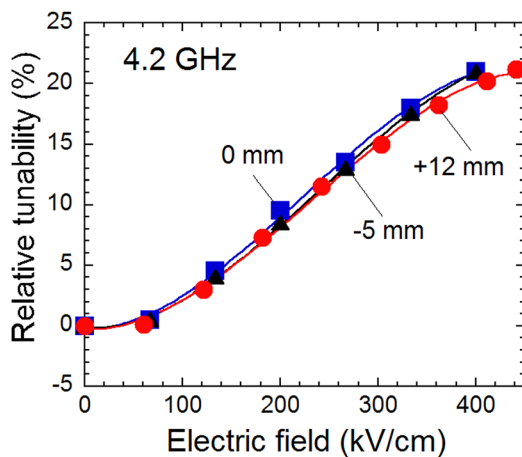


FIG. 7. Relative tunability of permittivity of the BF-BT films at 4.2 GHz vs. applied dc electric field for different coordinates  $x$ .

Fig. 8 shows the effective electromechanical coupling coefficients of the BAW resonators plotted versus relative tunability of permittivity of the BF-BT films for different coordinates  $x$ . The effective electromechanical coupling coefficient is calculated as

$$k_{\text{eff}}^2 = \frac{\pi^2 f_p - f_s}{4 f_p}, \quad (7)$$

where  $f_p$  and  $f_s$  are the parallel and series resonance frequencies determined at the maximum of the real parts of the complex impedance and admittance, respectively. The model of the field induced piezoelectric effect in a non-loaded ferroelectric film establishes following relationship between the electromechanical coupling factor  $k_f^2$  and the relative tunability of permittivity:<sup>15</sup>

$$k_f^2 \approx \frac{4q^2}{3c^0\beta} n_r = A_t n_r, \quad (8)$$

where  $q$ ,  $\beta$ , and  $c^0$  are the corresponding components of the tensors of linear electrostriction, dielectric nonlinearity, and elastic constant at zero dc electric field, respectively. The mechanical load by the electrodes reduces the electromechanical coupling due to the loss of acoustic energy in the non-piezoelectric electrodes.<sup>20,21</sup> However, the dc field dependence follows the same trend, i.e., the effective electromechanical coupling coefficient remains a linear function of the relative tunability of permittivity.<sup>20</sup> It can be seen from Fig. 8 that the measured dependences can be approximated by linear functions, which is in agreement with the model. Some nonlinearity appearing at the highest values of the relative tunability of permittivity can be explained by the fact that Eq. (8) is strictly valid in the limit of small tuning, i.e. small fields. Fig. 8 reveals that the slope of the coupling coefficient dependence on the relative tunability of permittivity increases with coordinate  $x$ . It results in larger coupling coefficients of the BAW resonators with the BF-BT films in the region facing the laser beam-plume interaction area. The reason for this is the higher proportionality coefficient  $A_t$  in Eq. (8). Since the dielectric responses of the test structures at

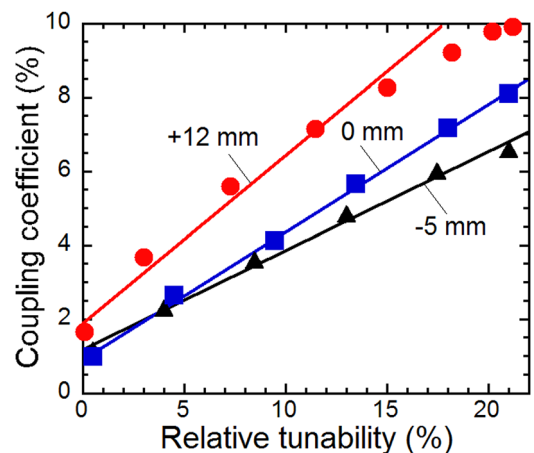


FIG. 8. Effective electromechanical coupling coefficient of the BAW resonators vs. relative tunability of permittivity of the BF-BT films for different coordinates  $x$ .

TABLE I. List of the tensor components of the linear electrostriction  $q$  and zero dc electric field elastic constant  $c^0$  for the BaTiO<sub>3</sub> of different orientations.<sup>15</sup>

Orientation	(100)	(110)	(111)
$q$ ( $\times 10^{10}$ m/F)	2.81	1.53	1.11
$c^0$ ( $\times 10^{11}$ N/m <sup>2</sup> )	2.55	2.77	2.84

different coordinates  $x$  are identical (see Fig. 7), the difference in the dielectric nonlinearity can be ignored. In accordance with our XRD analysis, the (100) BF-BT texturing increases with coordinate  $x$ . Therefore, the increase in the coefficient  $A_t$  can be associated with the anisotropy of the corresponding components of the tensors of linear electrostriction  $q$  and elastic constant  $c^0$ . The tensor components  $q$  and  $c^0$ , specific for different BF-BT orientations, are not available in the literature. The corresponding tensor components available for the BaTiO<sub>3</sub> of different orientations are listed in Table I (Ref. 15). As it can be seen from Table I, the elastic constant does not vary much with orientation. On the other hand, the linear electrostriction reveals rather strong anisotropy. In accordance with Eq. (8), the electromechanical coupling factor is proportional to square of the linear electrostriction constant. Therefore, one can conclude that the observed surface distribution of the effective electromechanical coupling coefficient is associated mainly with the anisotropy of the linear electrostriction constant  $q$ . The BF-BT film grains with (100) orientation reveal the largest  $q$ , which results in the largest effective electromechanical coupling coefficient of the BAW resonators (Fig. 8).

Fig. 9 shows the dc electric field dependence of the parallel resonance frequencies of the BAW resonators for different coordinates  $x$ . The difference in the resonance frequencies at zero dc field is less than 1%, which corresponds to tolerances in the BF-BT film thickness less than 10 nm. However, it can be seen that dependences are significantly different. Tunability of the parallel resonance frequency decreases with the coordinate  $x$ . In accordance with the model of the dc field induced piezoelectric effect (Ref. 15), the dc field dependent tunability of the parallel resonance frequency may be described in terms of the electromechanical coupling factor and relative tunability of permittivity as<sup>22</sup>

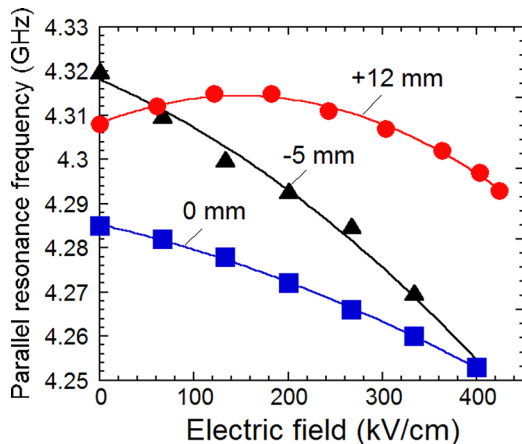


FIG. 9. Parallel resonance frequency of the BF-BT BAW resonators vs. applied dc electric field for different coordinates  $x$ .

$$n_{\text{pf}} = k_f^2 \left( \frac{m}{8q^2\varepsilon} + \frac{\varepsilon^b}{\varepsilon} \right) = n_r \left( \frac{m}{6c^0\beta\varepsilon} + A_t \frac{\varepsilon^b}{\varepsilon} \right), \quad (9)$$

where  $m$  and  $\varepsilon^b$  are the corresponding components of the tensors of nonlinear electrostriction and the background permittivity, respectively. The background permittivity comprises all nonferroelectric contributions to the permittivity of the material. For the BaTiO<sub>3</sub>, the background permittivity is estimated to be approximately 7.<sup>23</sup> Fig. 10 shows the tunability of the parallel resonance frequency of the BAW resonators plotted versus the relative tunability of permittivity of the BF-BT films for coordinates  $x = -5$  and  $+12$  mm. The tunability of the parallel resonance frequency is defined as

$$n_p = \frac{f_0 - f_p}{f_0}, \quad (10)$$

where  $f_0$  is the resonance frequency extrapolated to zero dc electric field. It can be seen that the tunability of parallel resonance frequency is lower in the film region facing the laser beam-plume interaction area and assumes even negative values. Analysis of Eq. (9) indicates that this behavior can be explained by an anisotropy of the components of the tensor of nonlinear electrostriction  $m$ . Again, keeping in mind that the (100) BF-BT texturing is enhanced in the “smooth” film region facing the laser beam-plume interaction, one can conclude that the  $m(100)$  component is negative and larger by absolute value than the  $m(110)$  and/or  $m(111)$  components.

Fig. 11 shows the dc electric field dependences of the series resonance frequency and its tunability of the BAW resonators for different coordinates  $x$ . The tunability of the series resonance frequency is defined in a similar way to that of the parallel resonance frequency (see Eq. (10)). It can be seen from Fig. 11 that the dependences are practically identical. In accordance with the model of the dc field induced piezoelectric effect (Ref. 15), the dc field dependent tunability of the series resonance frequency may be described in terms of the electromechanical coupling factor and relative tunability of permittivity as<sup>22</sup>

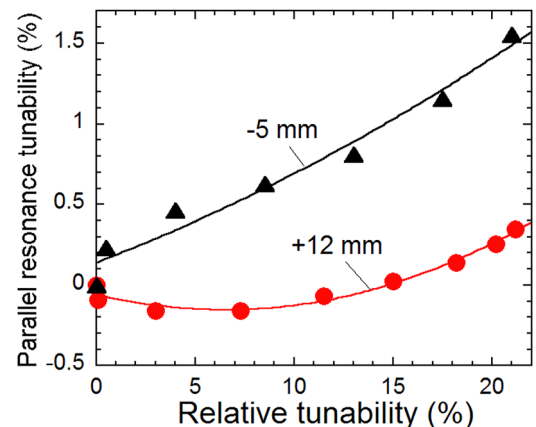


FIG. 10. Tunability of parallel resonance frequency of the BAW resonators vs. relative tunability of permittivity of the BF-BT films for different coordinates  $x$ .

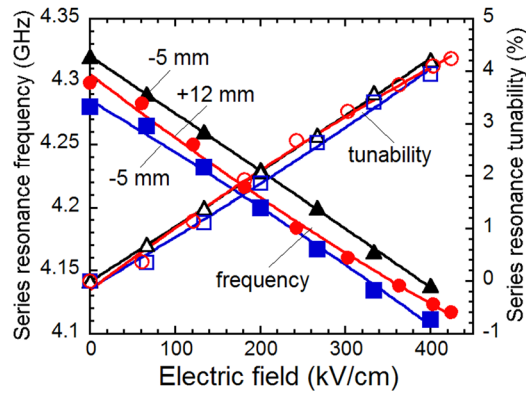


FIG. 11. Series resonance frequency and its tunability of the BF-BT BAW resonators vs. applied dc electric field for different coordinates  $x$ .

$$n_{sf} = k_f^2 \left( \frac{m}{8q^2 \varepsilon} + \frac{\varepsilon^b}{\varepsilon} + \frac{4}{\pi^2} \right) = n_r \left( \frac{m}{6c^0 \beta \varepsilon} + A_t \frac{\varepsilon^b}{\varepsilon} + A_t \frac{4}{\pi^2} \right). \quad (11)$$

The similarity of dependences shown in Fig. 11 can be explained by assuming that the effect of the negative and larger  $m(100)$  is compensated by larger coefficient  $A_t$  at the  $4/\pi^2$  term because of larger linear electrostriction constant (see Eq. (11)). An important conclusion is that the negative and larger nonlinear electrostriction constant, which is specific for the (100) BF-BT texturing, limits tunability of both parallel and series resonance frequencies.

#### IV. SUMMARY

It is demonstrated that there is a strong asymmetric surface distribution of the BF-BT film grain size, surface roughness and texturing relative to the laser plume axis in the PLD system. The grain size and surface roughness decrease significantly in the film region facing the laser beam-plume interaction area. The (100) BF-BT texturing enhances in that film region. The effect is explained by a reduction of the plume flow velocity, and, hence, reduction of the energy of species arriving at the condensation surface, which is caused by a higher plasma temperature and pressure in the part of the plume which absorbs the laser beam. In the “smooth” film region, the mechanical  $Q$ -factor of the BF-BT BAW resonators is up to 10 times higher. The rms surface roughness is, approximately, 35 nm and 15 nm, and  $Q$ -factor is 20 and 200, at resonance frequency of 4.2 GHz, in the “rough” and “smooth” film regions, respectively. The increase in the  $Q$ -factor is associated with a reduction of loss caused by wave scattering at reflection from the rough top interface. Simulations using the model of the roughness induced attenuation of the reflected acoustic waves indicate that in the “rough” film region the  $Q$ -factor is limited mainly by loss associated with wave scattering. The BF-BT BAW resonator tunable performance is analyzed using the theory of the dc field induced piezoelectric effect. The effective electromechanical coupling coefficient is, approximately, 7% and 10% in the “rough” and “smooth” film regions, respectively. The increase in the coupling coefficient is associated with the anisotropy of the components of the tensor of linear

electrostriction. The (100) oriented BF-BT grains reveal the largest linear electrostriction constant. Tunability of the parallel resonance frequency of the BF-BT BAW resonators is lower in the “smooth” film regions and assumes even negative values there. This is explained by anisotropy of the components of the tensor of nonlinear electrostriction. The (100) oriented BF-BT grains possess negative and larger, by absolute value, nonlinear electrostriction constant. The larger and negative nonlinear electrostriction constant limits the tunability of the series resonance frequency of the BF-BT BAW resonators in the “smooth” film regions on the level of 4.5%. The analysis of correlations between the PLD system configuration, BF-BT film microstructure, and acoustic performance of the BAW resonators allows for optimization of the deposition conditions and achieving the high resonator performance.

#### ACKNOWLEDGMENTS

This work was partly supported by the projects VR-FBAR, CompFBAR (Vetenskapsrådet) and NAFERBio (Vinnova), Sweden.

- <sup>1</sup>A. Noeth, T. Yamada, A. K. Tagantsev, and N. Setter, *J. Appl. Phys.* **104**, 094102 (2008).
- <sup>2</sup>S. A. Sis, V. Lee, J. D. Phillips, and A. Mortazawi, *IEEE MTT-S Int. Microwave Symp. Dig.* **2012**, 1.
- <sup>3</sup>G. N. Saddik, J. Son, S. Stemmer, and R. A. York, *J. Appl. Phys.* **109**, 091606 (2011).
- <sup>4</sup>A. Volatier, E. Defay, M. Aid, A. N'hari, P. Ancey, and B. Dubus, *Appl. Phys. Lett.* **92**, 032906 (2008).
- <sup>5</sup>B. Ivira, A. Reinhardt, E. Defay, and M. Aid, *IEEE Int. Freq. Control Symp. Dig.* **2008**, 254.
- <sup>6</sup>J. Berge and S. Gevorgian, *IEEE Trans. Ultrason. Ferroelectr. Freq. Control* **58**, 2768 (2011).
- <sup>7</sup>A. Vorobiev, S. Gevorgian, M. Löffler, and E. Olsson, *J. Appl. Phys.* **110**, 054102 (2011).
- <sup>8</sup>R. Aigner and L. Elbrecht, *RF Bulk Acoustic Wave Filters for Communications*, edited by K.-Y. Hashimoto (Artech House, Norwood, MA, 2009), p. 91.
- <sup>9</sup>A. Vorobiev, S. Gevorgian, N. Martirosyan, M. Löffler, and E. Olsson, *Appl. Phys. Lett.* **101**, 232903 (2012).
- <sup>10</sup>Z. Chen, D. Bleiner, and A. Bogaerts, *J. Appl. Phys.* **99**, 063304 (2006).
- <sup>11</sup>S. Mahieu, P. Ghekiere, D. Depla, and R. De Gryse, *Thin Solid Films* **515**, 1229 (2006).
- <sup>12</sup>A. Vorobiev, J. Berge, S. Gevorgian, M. Löffler, and E. Olsson, *J. Appl. Phys.* **110**, 024116 (2011).
- <sup>13</sup>A. Vorobiev and S. Gevorgian, *Int. J. Microwave Wireless Technol.* **5**, 361 (2013).
- <sup>14</sup>C. S. Hwang, M. D. Vaudin, and P. K. Schenck, *J. Mater. Res.* **13**, 368 (1998).
- <sup>15</sup>A. Noeth, T. Yamada, A. K. Tagantsev, and N. Setter, *J. Appl. Phys.* **104**, 094102 (2008).
- <sup>16</sup>A. Vorobiev and S. Gevorgian, *Appl. Phys. Lett.* **96**, 212904 (2010).
- <sup>17</sup>S. O. Leontsev and R. E. Eitel, *J. Am. Ceram. Soc.* **92**, 2957 (2009).
- <sup>18</sup>P. Padmini, T. R. Taylor, M. J. Lefevre, A. S. Nagra, R. A. York, and J. S. Speck, *Appl. Phys. Lett.* **75**, 3186 (1999).
- <sup>19</sup>S. G. Alekseev, G. D. Mansfel'd, N. I. Polzikova, and I. M. Kotelyanskii, *Acoust. Phys.* **53**, 465 (2007).
- <sup>20</sup>A. Noeth, T. Yamada, V. O. Sherman, P. Muralt, A. K. Tagantsev, and N. Setter, *J. Appl. Phys.* **102**, 114110 (2007).
- <sup>21</sup>S. Gevorgian and A. Vorobiev, in *Proceedings of the 40th European Microwave Conference, EuMC 2010; 13th European Microwave Week 2010, EuMW2010: Connecting the World, Paris, 28 September–30 September (2010)*, pp. 1210–1213.
- <sup>22</sup>A. Noeth, T. Yamada, P. Muralt, A. K. Tagantsev, and N. Setter, *IEEE Trans. Ultrason. Ferroelectr. Freq. Control* **57**, 379 (2010).
- <sup>23</sup>J. Hlinka and P. Marton, *Phys. Rev. B* **74**, 104104 (2006).